Pharmacological Research 187 (2023) 106589

Contents lists available at ScienceDirect

Pharmacological Research

journal homepage: www.elsevier.com/locate/yphrs

Inhibition of Rho-kinase ameliorates decreased spine density in the medial prefrontal cortex and methamphetamine-induced cognitive dysfunction in mice carrying schizophrenia-associated mutations of the *Arhgap10* gene

Rinako Tanaka [a,1], Jingzhu Liao [a,1], Kazuhiro Hada [a,1], Daisuke Mori [b], Taku Nagai [a,c], Tetsuo Matsuzaki [a], Toshitaka Nabeshima [d,e], Kozo Kaibuchi [f,g], Norio Ozaki [b], Hiroyuki Mizoguchi [a], Kiyofumi Yamada [a,e,*,2]

[a] Department of Neuropsychopharmacology and Hospital Pharmacy, Nagoya University Graduate School of Medicine, Nagoya, Aichi 466-8560, Japan
[b] Department of Psychiatry, Nagoya University Graduate School of Medicine, Nagoya, Aichi 466-8560, Japan
[c] Division of Behavioral Neuropharmacology, International Center for Brain Science (ICBS), Fujita Health University, Toyoake, Aichi 470-1192, Japan
[d] Laboratory of Health and Medical Science Innovation, Fujita Health University Graduate School of Health Sciences, Toyoake, Aichi 470-1192, Japan
[e] Japanese Drug Organization of Appropriate Use and Research, Nagoya, Aichi 468-0069, Japan
[f] Department of Cell Pharmacology, Nagoya University Graduate School of Medicine, Nagoya, Aichi 466-8560, Japan
[g] International Center for Brain Science, Fujita Health University, Toyoake, Aichi 470-1129, Japan

ARTICLE INFO

Keywords:
CNV
C-Fos
MYPT1
ROCK
Small GTPase

Chemical compounds studied in this article:
fasudil monohydrochloride salt (PubChem CID: 163751)
methamphetamine (PubChem CID: 10836)

ABSTRACT

Copy-number variations in the *ARHGAP10* gene encoding Rho GTPase–activating protein 10 are associated with schizophrenia. Model mice (*Arhgap10* S490P/NHEJ mice) that carry "double-hit" mutations in the *Arhgap10* gene mimic the schizophrenia in a Japanese patient, exhibiting altered spine density, methamphetamine-induced cognitive dysfunction, and activation of RhoA/Rho-kinase signaling. However, it remains unclear whether the activation of RhoA/Rho-kinase signaling due to schizophrenia-associated *Arhgap10* mutations causes the phenotypes of these model mice. Here, we investigated the effects of fasudil, a brain permeable Rho-kinase inhibitor, on altered spine density in the medial prefrontal cortex (mPFC) and on methamphetamine-induced cognitive impairment in a touchscreen-based visual discrimination task in *Arhgap10* S490P/NHEJ mice. Fasudil (20 mg/kg, intraperitoneal) suppressed the increased phosphorylation of myosin phosphatase–targeting subunit 1, a substrate of Rho-kinase, in the striatum and mPFC of *Arhgap10* S490P/NHEJ mice. In addition, daily oral administration of fasudil (20 mg/kg/day) for 7 days ameliorated the reduced spine density of layer 2/3 pyramidal neurons in the mPFC. Moreover, fasudil (3–20 mg/kg, intraperitoneal) rescued the methamphetamine (0.3 mg/kg)-induced cognitive impairment of visual discrimination in *Arhgap10* S490P/NHEJ mice. Our results suggest that Rho-kinase plays significant roles in the neuropathological changes in spine morphology and in the vulnerability of cognition to methamphetamine in mice with schizophrenia-associated *Arhgap10* mutations.

1. Introduction

Schizophrenia is a severe psychiatric disorder that typically emerges in late adolescence and early adulthood [1]. It affects approximately 1 % of the population and involves positive symptoms (such as hallucinations and delusions), negative symptoms (such as flat affect and social withdrawal), and cognitive dysfunction (such as deteriorations in working memory, executive function, and learning) [2]. The

Abbreviations: ANOVA, analysis of variance; CNVs, copy number variations; i.p., intraperitoneal; MLC, myosin light chain; mPFC, medial prefrontal cortex; MYPT1, myosin phosphatase–targeting subunit 1; NAc, nucleus accumbens; NeuN, neuronal nuclei; NHEJ, non-homologous end-joining; NMDA-Rs, N-methyl-D-aspartate receptors; PB, phosphate buffer; PBS, phosphate-buffered saline; PFA, paraformaldehyde; PFC, prefrontal cortex; pMYPT1, phosphorylated MYPT1; ROI, region of interest; WT, wild-type.

* Correspondence to: 65 Tsurumai, Showa, Nagoya, Aichi 466-8560, Japan.
E-mail address: kyamada@med.nagoya-u.ac.jp (K. Yamada).
[1] Rinako Tanaka, Jingzhu Liao, and Kazuhiro Hada contributed equally to this work.
[2] ORCID: http://orcid.org/0000-0002-5280-5180

https://doi.org/10.1016/j.phrs.2022.106589
Received 26 October 2022; Received in revised form 22 November 2022; Accepted 28 November 2022
Available online 30 November 2022

pathoetiology of schizophrenia is not yet fully understood because of its complexity and heterogeneity. It is generally accepted, however, that both genetic vulnerability and environmental risk factors are involved in its development (dual-hit hypothesis) [3]. Several copy-number variations (CNVs) such as 1q21.1, 2p16.3 (*NRXN1*), 3q29, 15q11.2, 15q13.3, and 22q11.2 have been consistently reported to be associated with the genetic risk of schizophrenia [4,5]. Environmental risks include perinatal maternal infection or stress and the administration of cannabis or methamphetamine [6,7]. In addition, psychostimulants, including amphetamine and methamphetamine, can cause psychotic symptoms and cognitive dysfunction in schizophrenia patients at doses that show little effect in healthy controls [8–10].

Cognitive dysfunction emerges before the first episode of psychosis and is regarded as a potential predictor of functional recovery in patients with schizophrenia [11–13]. Although cognitive dysfunction is present in over 80% of patients with schizophrenia, it is not well controlled by current antipsychotic drugs such as antagonists of the dopamine D_2 receptor or serotonin 5-HT_{2A} receptor [14]. Cognitive dysfunction in schizophrenia is considered to be associated with synaptic dysfunction in cortical regions [15]. Patients with schizophrenia exhibit decreased gray matter volume in the frontal cortex and a reduced density of spines, a component of the postsynaptic site of most excitatory synapses, in pyramidal neurons of the prefrontal cortex (PFC) [15–19]. Furthermore, schizophrenia patients show reductions in both PFC blood flow and functional connectivity between the PFC and other brain regions when performing a cognitive task [20]. Thus it is necessary to explore new therapeutic targets for schizophrenia that focus on synaptic dysfunction in the PFC to improve cognitive function in schizophrenia patients.

We recently identified a significant association between schizophrenia and CNVs in the *ARHGAP10* gene encoding Rho GTPase–activating protein 10 [21]. We focused on one schizophrenia patient with "double-hit" mutations in *ARHGAP10*: a missense (p.S490P) variation in exon 17 and an exonic deletion on the other allele. The patient has had low academic performance and a poor response to pharmacotherapy regarding both positive and negative symptoms. To mimic this case, we established novel *Arhgap10* S490P/NHEJ mice carrying a double-hit involving 2 mutations: a missense variant (p.S490P) and a frameshift mutation caused by non-homologous end-joining (NHEJ) [21]. Through comprehensive behavioral and neuropathological examinations, we determined that these mice had reduced spine density in layer 2/3 pyramidal neurons of the medial PFC (mPFC) and a vulnerability to methamphetamine-induced cognitive dysfunction in a visual discrimination task after treatment with methamphetamine at a dose that had no effect on visual discrimination in wild-type (WT) mice [21,22].

ARHGAP10 is a Rho GTPase–activating protein that inactivates RhoA/Rho-kinase signaling by converting the GTP-bound form of RhoA to the GDP-bound form [23,24]. The ARHGAP10 p.S490P mutant showed significantly less interaction with constitutively active RhoA compared with WT ARHGAP10 [21]. In addition, the phosphorylation levels of myosin phosphatase–targeting subunit 1 (MYPT1), one of the major substrates of Rho-kinase, were increased in the striatum and nucleus accumbens (NAc) of *Arhgap10* S490P/NHEJ mice compared with WT littermates [22]. These data suggest that the double-hit mutations in *ARHGAP10* that were identified in one schizophrenia patient resulted in the activation of RhoA/Rho-kinase signaling in the brains of *Arhgap10* S490P/NHEJ mice. It should be noted that activation of RhoA in neurons leads to spine loss and shrinkage as a result of Rho-kinase regulation of actin cytoskeletal dynamics [25–27]. Accordingly, we hypothesized that activation of RhoA/Rho-kinase signaling due to the double-hit mutations in *Arhgap10* may be associated with the reduced mPFC spine density and the cognitive impairment in *Arhgap10* S490P/NHEJ mice. To test this hypothesis, we investigated the effect of fasudil, a brain-permeable Rho-kinase inhibitor, on the decreased spine density of cortical neurons in the mPFC and the methamphetamine-induced impairment of the visual discrimination task in *Arhgap10* S490P/NHEJ mice.

2. Materials and methods

2.1. Animals

Arhgap10 S490P/NHEJ mutant mice (NHEJ and S490P line) were generated on a C57BL/6 J genetic background as described previously [21]. *Arhgap10* S490P/NHEJ (n = 85) mice and their WT littermates (n = 57) were obtained by breeding 2 lines of heterozygous *Arhgap10* mutant mice (NHEJ line and S490P line). Male mice aged 7–15 weeks old were used in the experiment. Mice were housed at a density of 4–6 mice per cage (28 cm length × 17 cm width × 13 cm high) in standard conditions (23 ± 1 °C, 50 ± 5 % humidity) with a 12-h light/dark cycle. Food and water were available ad libitum. Animals were handled in accordance with the guidelines established by the Institutional Animal Care and Use Committee of Nagoya University, the Guiding Principles for the Care and Use of Laboratory Animals approved by the Japanese Pharmacological Society, and the National Institutes of Health Guide for the Care and Use of Laboratory Animals.

2.2. Antibodies

For western blotting, the primary antibodies used were as follows: rabbit anti-MYPT1 (Cat# 2634, RRID:AB_915965, 1:1000; Cell Signaling Technology, Danvers, MA, USA) and rabbit anti–phospho-MYPT1 (Thr696) (Cat# ABS45, RRID:AB_10562238, 1:1000; Millipore, Darmstadt, Germany). The secondary antibodies were horseradish peroxidase–conjugated anti–rabbit IgG antibody (Cat# NA9340, RRID:AB_772191, 1:10,000; GE Healthcare, Chicago, IL, USA). For immunohistochemistry, the primary antibodies used were as follows: rabbit anti–phospho-MYPT1 (Thr696) (Cat# ABS45, RRID:AB_10562238, 1:100; Millipore), rabbit anti–c-Fos (Cat# sc-7202, RRID:AB_2106765, 1:1000 dilution; Santa Cruz Biotechnology, Dallas, TX, USA), and mouse anti–neuronal nuclei (NeuN) (Cat# MAB377, RRID:AB_2298772, 1:500 dilution; Millipore). The secondary antibodies were goat anti–mouse Alexa Fluor 488 (Cat# A11029, RRID:AB_ 2534088, 1:1000 dilution; Thermo Fisher Scientific, Waltham, MA, USA), goat anti–rabbit Alexa Fluor 594 (Cat# A11037, 1:1000 dilution, RRID:AB_ 2534095; Thermo Fisher Scientific), goat anti–rabbit Alexa Fluor 488 (Cat# A11034, RRID:AB_2576217, 1:1000 dilution; Thermo Fisher Scientific), and goat anti–mouse Alexa Fluor 568 (Cat# A11031, 1:1000 dilution, RRID:AB_144696; Thermo Fisher Scientific).

2.3. Drug treatment

Fasudil monohydrochloride salt (purity > 99 %) was kindly supplied by Asahi Kasei Pharma (Tokyo, Japan). In our previous study, fasudil and its major active metabolite, hydroxyfasudil, were detected in the brain at concentrations over their respective Ki values for Rho-kinase after intraperitoneal (i.p.) injection of 10 mg/kg fasudil in C57BL/6 J mice. Following oral administration, brain hydroxyfasudil was detected at concentrations over the Ki value for Rho-kinase while fasudil was undetectable [28]. Accordingly, we set up the dose and timing of fasudil administration as follows. To evaluate the phosphorylation levels of MYPT1 via western blotting and immunohistochemistry, fasudil (20 mg/kg) or vehicle was administrated intraperitoneally 60 min before sample collection. For Golgi staining, mice were orally treated with fasudil (20 mg/kg) or vehicle once a day for 7 days in order to detect the effect on spine density, because spine turnover is reported to occur 2 days in adult mice [19,29]. We chose oral administration of fasudil once a day to minimize injection-related stress. On the day after the last fasudil administration we collected brain samples for Golgi staining. For the visual discrimination task, fasudil (3–20 mg/kg) or vehicle was administrated intraperitoneally 5 min before the task, and methamphetamine (Sumitomo Dainippon Pharma, Osaka, Japan) (0.3 mg/kg) or

vehicle was administrated intraperitoneally 30 min before the task. For c-Fos expression analysis, methamphetamine (0.3 mg/kg) and fasudil (20 mg/kg) were administrated intraperitoneally 150 min and 125 min before perfusion, respectively, according to the schedule of the visual discrimination task.

2.4. Western blotting

We used 10- to 15-week-old mice. Western blotting was performed as described previously [22]. In brief, tissue from the striatum, NAc, and mPFC was dissected from mouse brains according to the mouse brain atlas (Franklin and Paxinos, 1997), using 2-mm-diameter biopsy punches (Cat# 52–004620, Integra Miltex; Davies Dr, York, PA, USA). The tissue was lysed by lysis buffer (complete protease inhibitor cocktail (Cat# 11873580001; Roche, Basel, Switzerland), and phosSTOP phosphatase inhibitors (Cat# 4906837001; Roche) in 1% SDS solution). Then the tissue was immediately sonicated and heated at 99 °C for 10 min. Lysates were centrifuged at 15,000 × *g* for 15 min. The protein concentration was determined using a DC Protein Assay Kit (Cat# 5000111JA; Bio-Rad Laboratories, Hercules, CA, USA), and protein was diluted in sample buffer (0.5 M Tris-HCl, pH 6.8, 1% SDS, 30% glycerol, 0.0012% bromophenol blue, and 0.93% DTT). Samples were applied to an 8% SDS-polyacrylamide gel and subsequently transferred to a polyvinylidene difluoride membrane (Cat# IPVH00010; Millipore). The membranes were blocked with Blocking One-P (Cat# 05999–84; Nacalai Tesque, Kyoto, Japan) at room temperature for 1 h and incubated with a primary antibody at 4 °C overnight. Then, membranes were washed three times every 10 min with 0.05% Tween 20 in tris-buffered saline. After incubation with horseradish peroxidase–conjugated secondary antibody at room temperature for 1 h, the immune complex was detected using ECL Prime Western Blotting Detection Reagents (Cat# RPN2236; GE Healthcare). The intensities of the bands on the membranes were analyzed using LuminoGraph I (Atto Instruments, Tokyo, Japan). To calculate the relative amount of phosphorylated proteins compared with total proteins, the same membranes were stripped with WB Stripping Solution Strong (Cat# 05677–65; Nacalai Tesque) at room temperature for 1 h and treated as described above. All data from western blotting were expressed as relative fold change in expression compared to control. The primary and secondary antibody was diluted with Can Get Signal Solutions 1 and 2 (Cat# NKB-101; Toyobo, Osaka, Japan), respectively, to enhance antibody–antigen binding.

2.5. Immunohistochemistry

We used 10- to 15-week-old mice. Immunohistochemistry was conducted as described previously [30] with minor modifications. In the immunohistochemical analysis of pMYPT1 and NeuN, mice were perfused intracardially with ice-cold 4 % paraformaldehyde (PFA) in 0.1 M phosphate buffer (PB) (pH 7.4) at a rate of 10 mL/min for 6 min under anesthesia with medetomidine, midazolam, and butorphanol. In the immunohistochemical analysis of c-Fos, mice were perfused intracardially with ice-cold 0.1 M PB followed by 4 % PFA in 0.1 M PB under anesthesia with isoflurane. The brains were post-fixed with the same fixative and cryoprotected with 20 % sucrose followed by 30 % sucrose in 0.1 M PB. Frozen 20-μm sections for the immunohistochemical analysis of pMYPT1 and NeuN, or 30-μm sections for the immunohistochemical analysis of c-Fos, were cut coronally using a cryostat (CM3050S; Leica, Wetzlar, Germany). Cryosections were fixed with 4 % paraformaldehyde in 0.1 M PB for 5 min and permeabilized with 0.3% Triton X-100 / phosphate-buffered saline (PBS) for 10 min. After incubation in blocking solution (5% goat serum / PBS with 0.3% Triton X-100) for 60 min, the sections were immunostained overnight with the primary antibody. After washing in PBS, the sections were incubated with the secondary antibody at room temperature for 1 h. After washing in PBS, the sections were mounted on an adhesive silane (MAS) –coated glass slide (Matsunami, Osaka, Japan) with Fluorescent Mounting Medium (Dako, Santa Clara, CA, USA) and a coverslip. Fluorescent images were captured using a confocal laser microscope (LSM710; Carl Zeiss AG, Oberkochen, Germany). The mPFC and striatum were identified according to the mouse brain atlas (Franklin and Paxinos, 1997). For quantitative analysis of immunohistochemistry, one region of interest (ROI) per slice × 3 slices in each brain region were used in each mouse. The number of positive cells was counted within each 93 μm × 93 μm ROI for the immunohistochemical analysis of pMYPT1 and NeuN, or each 320 μm × 320 μm ROI for the analysis of c-Fos immunohistochemistry, using Metamorph software (Molecular Devices, Sunnyvale, CA, USA). We defined positive cells as those with a signal intensity above the background threshold.

2.6. Golgi staining

We used 7- to 8-week-old mice. Golgi staining was carried out using the FD Rapid Golgi Stain Kit (FD NeuroTechnologies, Ellicott City, MD, USA) and the methods described in a previous study [22]. The cryosections were sliced at 80 μm using a cryostat. We obtained the images of layer 2/3 pyramidal neurons in the mPFC by BZ9000 bright-field microscopy (KEYENCE, Hyogo, Japan) using an oil-immersion 100 × objective lens. Only fully impregnated neurons isolated from neighboring impregnated neurons were retained for analyses. We quantified the spine density of dendrites 50–200 μm from the soma of pyramidal neurons (6–7 dendrites per mouse). Spine density was expressed as the number of spines per 10 μm of dendrite length. All dendrites and spines were traced in images using Neurolucida software (MicroBrightField Bioscience, Williston, VT, USA) and analyzed using NeuroExplorer (MicroBrightField Bioscience).

2.7. Touchscreen-based visual discrimination task

The protocol was described in previous reports [22]. Briefly, in order to create enough motivation to perform the task, 8-week-old mice were restricted in their access to food and water to 2 h per day (5:00–7:00 pm) at least 1 week before the pretraining, with the goal of achieving approximately 85–95% of the bodyweight they attained on an ad libitum diet. The food and water restriction was continued until the end of the task. The task started with 5 pre-training steps (habituation, initial touch, must touch, must initiate, and punish incorrect) to shape screen-touching behavior. After mice completed this pre-training ($\geq$ 75% correct responses for 2 consecutive days), they subsequently performed the visual discrimination task, in which trial initiation was triggered by their touching the nozzle, and 2 stimuli (marble and fan) were then presented simultaneously in the 2 response windows. Touching the correct window resulted in the delivery of a liquid reward (20 μl). When the incorrect window was touched, the stimuli offset immediately and a 5-s time-out period was started. After an inter-trial interval (20 s), a correction trial was given instead of a new trial. In the correction trial, the same stimulus set was repeatedly presented in the same location until the mouse made a correct response. Stimulus contingencies were counterbalanced. The session finished after 1 h or 30 trials were completed, whichever came first. The total number of trials, total number of correction trials, response latencies, percentage of trials completed, number of correction errors, and percentage of correct responses were analyzed. When mice could achieve $\geq$ 80% correct responses for 2 consecutive days, the final stage, namely the visual discrimination task with drug treatment, was begun. In this stage, the initial acquisition and the contingency of the stimulus pair were similar to those of the of the visual discrimination task and methamphetamine or fasudil was administered in a crossover design considering the counterbalance.

2.8. Statistical analysis

All data are expressed as mean ± SEM. Statistical analyses were

performed with GraphPad Prism 9 (RRID:SCR_002798; GraphPad Software, San Diego, CA, USA). The Brown–Forsythe test was used to test for the equality of group variances. Statistical significance ($P < 0.05$) was determined using two-way analysis of variance (ANOVA), mixed-effects analysis, or the Kruskal-Wallis test for multigroup comparisons. Tukey's multiple comparison test or Dunn's multiple comparisons test was used for post hoc comparison. The sample size for each experiment was determined based on our previous studies using the relevant type of experiment [21,22]. Detailed information concerning statistical analysis is shown in Table S1.

3. Results

3.1. The effect of fasudil on Rho-kinase activity in the brain of Arhgap10 S490P/NHEJ mice

ARHGAP10 regulates RhoA activity by transforming the GTP-binding form (active form) of RhoA to its GDP-binding form (inactive form) [23,24]. Rho-kinase, an effector of RhoA, catalyzes the phosphorylation of MYPT1 at Thr696, thereby regulating the phosphorylation levels of myosin light chain (MLC) [25,31,32]. Our previous study indicated that the phosphorylated MYPT1 (pMYPT1) levels in the striatum and NAc in *Arhgap10* S490P/NHEJ mice were higher than those in WT mice, whereas there were no differences in total MYPT1 levels between the 2 groups of mice [22]. These findings raised the possibility that RhoA/Rho-kinase signaling is activated in the brain of *Arhgap10* S490P/NHEJ mice. To test this possibility, we investigated the effect of fasudil, a brain-permeable Rho-kinase inhibitor, on the increased pMYPT1 levels in *Arhgap10* S490P/NHEJ mice. Consistent with our previous study [22], pMYPT1 (Thr696) levels in the striatum and NAc were significantly higher in *Arhgap10* S490P/NHEJ mice than in WT mice, even after saline injection. Fasudil (20 mg/kg, i.p.) suppressed pMYPT1 (Thr696) levels in the striatum and NAc in *Arhgap10* S490P/NHEJ mice but had no effect in WT mice (Fig. 1A, B, D, E) (Figs. 1B, 2-way ANOVA, genotype: $F(1, 36) = 27.31$, $P < 0.0001$, fasudil: $F(1, 36) = 5.175$, $P = 0.0290$, genotype × fasudil: $F(1, 36) = 3.719$, $P = 0.0617$; Figs. 1E, 2-way ANOVA, genotype: $F(1, 36) = 16.37$, $P = 0.0003$, fasudil: $F(1, 36) = 16.58$, $P = 0.0002$, genotype × fasudil: $F(1, 36) = 5.208$, $P = 0.0285$). On the other hand, in the mPFC there were no differences in pMYPT1 (Thr696) levels between *Arhgap10* S490P/NHEJ and WT mice and they were not affected by fasudil (Fig. 1G, H) (Figs. 1H, 2-way ANOVA, genotype: $F(1, 36) = 0.08369$, $P = 0.7740$, fasudil: $F(1, 36) = 3.885$, $P = 0.0565$, genotype × fasudil: $F(1, 36) = 0.4716$, $P = 0.4966$). In all regions, total MYPT1 levels showed no differences between groups (Fig. 1C, F, I) (Fig. 1C, 2-way ANOVA, genotype: $F(1, 36) = 0.6972$, $P = 0.4092$, fasudil: $F(1, 36) = 3.474$, $P = 0.0705$, genotype × fasudil: $F(1, 36) = 13.28$, $P = 0.0008$; Fig. 1 F, 2-way ANOVA, genotype: $F(1, 36) = 0.2016$, $P = 0.6561$, fasudil: $F(1, 36) = 0.3330$, $P = 0.5675$, genotype × fasudil: $F(1, 36) = 1.238$, $P = 0.2733$; Figs. 1I, 2-way ANOVA, genotype: $F(1, 36) = 2.064$, $P = 0.1594$, fasudil: $F(1, 36) = 0.01162$, $P = 0.9147$, genotype × fasudil: $F(1, 36) = 4.692$, $P = 0.0370$).

Although western blotting showed that the mPFC of *Arhgap10* S490P/NHEJ mice exhibited no changes in pMYPT1 levels or any effect of fasudil, we considered that immunohistochemical analysis might detect subtle changes in pMYPT1 levels in the mPFC. pMYPT1 (Thr696) signals were detectable in about 97% of NeuN-positive neurons in the mPFC regardless of genotype and fasudil treatment (Fig. 2A, B). The ratio of pMYPT1 (Thr696) and NeuN double-positive neurons to NeuN-positive neurons in the mPFC was significantly higher in *Arhgap10* S490P/NHEJ mice than in WT mice. Fasudil (20 mg/kg, i.p.) suppressed the ratio of pMYPT1 (Thr696) to NeuN-positive neurons in the mPFC of *Arhgap10* S490P/NHEJ mice but had no effect in WT mice (Fig. 2A, C) (Fig. 2C, genotype: $F(1, 56) = 5.138$, $P = 0.0273$, fasudil: $F(1, 56) = 20.75$, $P < 0.0001$, genotype × fasudil: $F(1, 56) = 4.424$, $P = 0.0400$). These results provide further support for our hypothesis that RhoA/Rho-kinase signaling is activated in the striatum, NAc, and mPFC of *Arhgap10* S490P/NHEJ mice. Accordingly, we considered that the inhibition of Rho-kinase by fasudil reduced pMYPT1 levels in each of these regions of *Arhgap10* S490P/NHEJ mice.

3.2. The effect of fasudil on spine density in the mPFC of Arhgap10 S490P/NHEJ mice

We previously reported decreased spine density of layer 2/3 pyramidal neurons in the mPFC of *Arhgap10* S490P/NHEJ mice [21]. RhoA/Rho-kinase signaling promotes spine shrinkage and destabilization through regulation of actin dynamics [26,27]. To explore a possible role of Rho-kinase in the altered spine density of *Arhgap10* S490P/NHEJ mice, we investigated whether fasudil ameliorated the abnormal spine density in the mPFC of *Arhgap10* S490P/NHEJ mice. Golgi staining confirmed our previous data [21] that the spine density of pyramidal neurons in layer 2/3 of the mPFC was significantly decreased in *Arhgap10* S490P/NHEJ mice compared with WT mice. Daily oral administration of fasudil (20 mg/kg/day) for 7 days restored the decreased spine density of layer 2/3 pyramidal neurons in the mPFC of *Arhgap10* S490P/NHEJ mice, although it had no effect on the spine density in WT mice (Fig. 3A, B) (Figs. 3B, 2-way ANOVA, genotype: $F(1, 118) = 10.26$, $P = 0.0017$, fasudil: $F(1, 118) = 20.96$, $P < 0.0001$, genotype × fasudil: $F(1, 118) = 9.221$, $P = 0.0029$). This result suggests that the abnormal activation of Rho-kinase in *Arhgap10* S490P/NHEJ mice contributes to decreased spine density in the mPFC.

3.3. The effect of fasudil on methamphetamine-induced impairment of visual discrimination in Arhgap10 S490P/NHEJ mice

We previously reported that *Arhgap10* S490P/NHEJ mice showed impairment in the touchscreen–based visual discrimination task after pretreatment with methamphetamine at a dose of 0.3 mg/kg, although the same treatment had no effect on WT mice. Furthermore, *Arhgap10* S490P/NHEJ and WT mice treated with methamphetamine at a dose of 0.3 mg/kg showed no differences in the amounts of time required to make correct responses or to retrieve rewards in the visual discrimination task. Thus, the mutant mice were vulnerable to methamphetamine treatment in terms of cognitive function, but not motor function [22]. This phenotype in *Arhgap10* S490P/NHEJ mice may be consistent with that in schizophrenia patients, whose symptoms are exacerbated by psychostimulant drugs [8,9]. To evaluate the potential role of Rho-kinase on methamphetamine-induced cognitive impairment in *Arhgap10* S490P/NHEJ mice, we investigated the effect of fasudil on the reduced visual discrimination caused by methamphetamine after the mutant mice exhibited stable discrimination performance (≥ 80 % correct responses) for 2 consecutive days (Fig. 4A). Methamphetamine (0.3 mg/kg) treatment decreased the percentage of correct responses in *Arhgap10* S490P/NHEJ mice (Fig. 4B) (mixed-effects analysis: $F(2.942, 22.95) = 10.06$, $P = 0.0002$), and also decreased the number of total normal correct trials but increased the number of total error trials (Fig. 4C, D) (Fig. 4 C, mixed-effects analysis: $F(2.712, 21.16) = 8.836$, $P = 0.0007$; Fig. 4D, mixed-effects analysis: $F(2.763, 21.55) = 9.779$, $P = 0.0004$). Fasudil (3–20 mg/kg, i.p.) partially reversed the decreases in the correct response rate (Fig. 4B) and total normal correct trials (Fig. 4C), as well as the increase in the total normal error trials (Fig. 4D), in the visual discrimination task in methamphetamine-treated *Arhgap10* S490P/NHEJ mice. On the other hand, the completion time and the percentage of mice that completed 30 trials within 60 min were comparable between saline- and methamphetamine-treated *Arhgap10* S490P/NHEJ mice, and fasudil had little effect on these indices (Fig. 4E, F) (Fig. 4E, mixed-effects analysis: $F(2.268, 17.69) = 3.357$, $P = 0.0531$). We confirmed that in saline-treated WT mice, fasudil at a dose of 20 mg/kg did not affect the percentage of correct responses, the number of total normal correct trials and total normal error trials, or the completion time [33]. These results suggest that Rho-kinase is

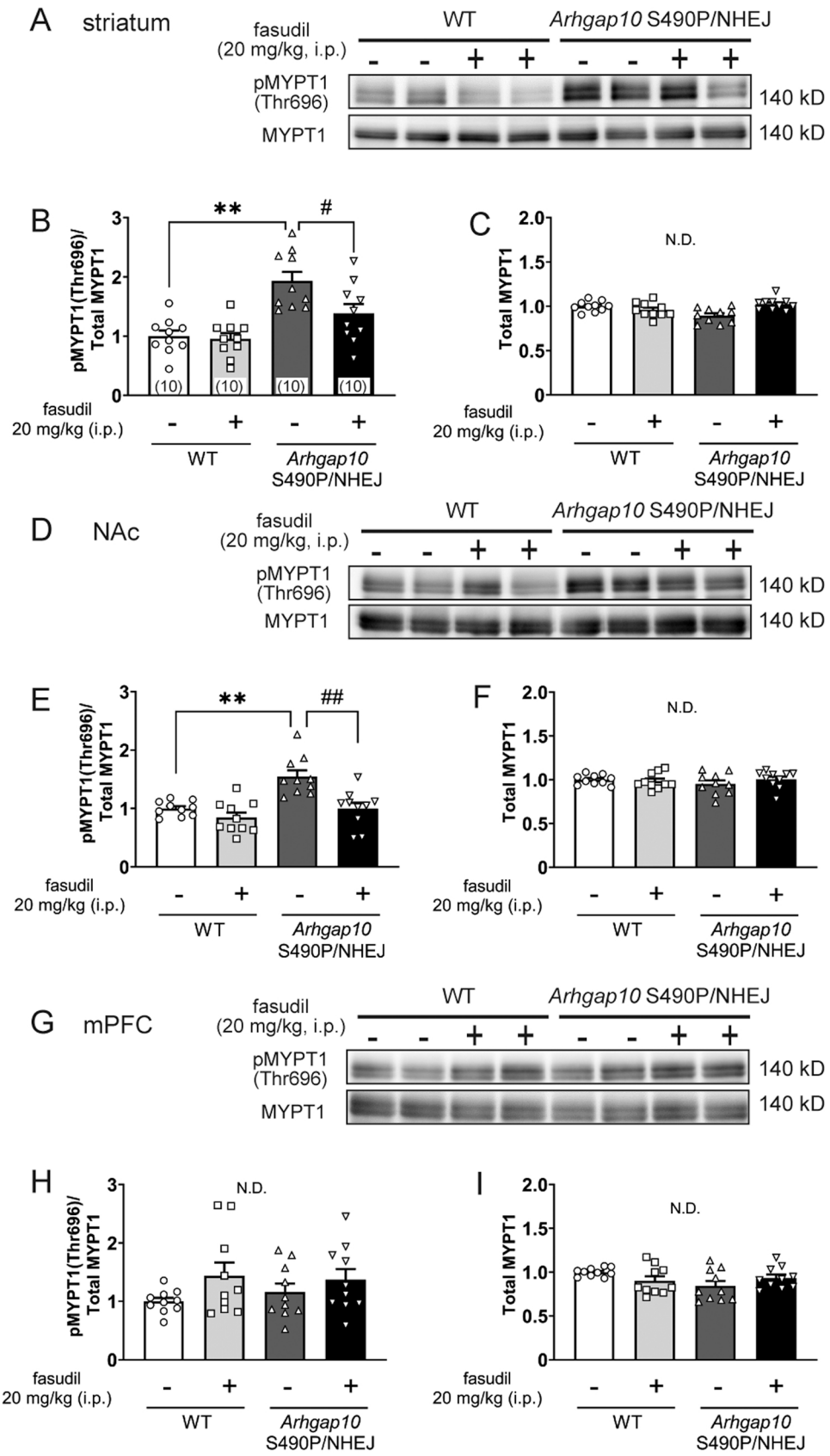

Fig. 1. The effect of fasudil on phosphorylation levels of MYPT1 at Thr696 in *Arhgap10* S490P/NHEJ mice. A, D, G: Western blotting of pMYPT1 (Thr696) and total MYPT1 in the striatum (A), NAc (D), and mPFC (G). B, E, H: Ratios of pMYPT1 (Thr696) levels to total MYPT1 levels in the striatum (B), NAc (E), and mPFC (H) of *Arhgap10* S490P/NHEJ mice or WT mice 60 min after fasudil (20 mg/kg, i.p.) treatment. C, F, I: Quantification of total MYPT1 levels in the striatum (C), NAc (F), and mPFC (I) of *Arhgap10* S490P/NHEJ mice or WT mice 60 min after fasudil (20 mg/kg, i.p.) treatment. Data represent the mean ± SEM (n = 10 mice per group) and were analyzed by Tukey's multiple comparison test. * *$P < 0.01$ compared with WT mice and $^{\#}P < 0.05$, $^{\#\#}P < 0.01$ compared with the vehicle group.

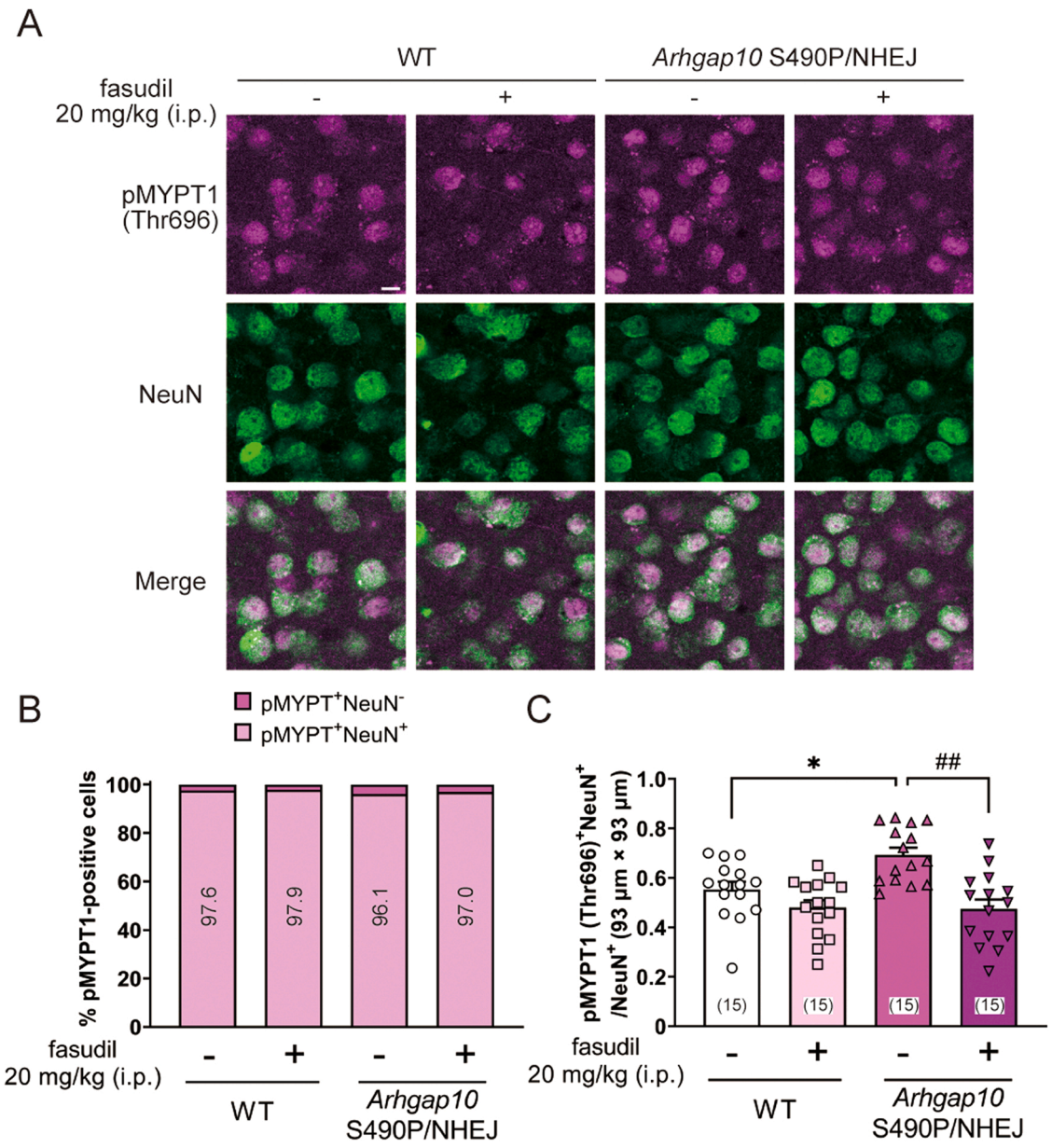

Fig. 2. The effect of fasudil on expression levels of pMYPT1 (Thr696) on NeuN-positive neurons in the mPFC of *Arhgap10* S490P/NHEJ mice. A. Representative images of pMYPT1 (Thr696) (magenta) and NeuN (green) immunoreactivity in the mPFC of *Arhgap10* S490P/NHEJ mice (scale bar indicates 10 µm). B. Percentage of pMYPT1 (Thr696)-positive cells co-localized with NeuN-positive neurons in *Arhgap10* S490P/NHEJ mice or WT mice 60 min after fasudil (20 mg/kg, i.p.) treatment. C. Ratio of pMYPT1 (Thr696) and NeuN double-positive neurons to NeuN-positive neurons in the mPFC of *Arhgap10* S490P/NHEJ mice or WT mice 60 min after fasudil (20 mg/kg, i.p.) treatment. Data represent the mean ± SEM (n = 15 slices in each of 5 mice per group (3 slices per mouse)) and were analyzed by Tukey's multiple comparison test. *$P < 0.05$ compared with WT mice and $^{\#\#}P < 0.01$ compared with the vehicle group.

associated with the methamphetamine-induced cognitive impairment seen in the visual discrimination task in *Arhgap10* S490P/NHEJ mice.

3.4. The effect of fasudil on the neuronal activation induced by methamphetamine in Arhgap10 S490P/NHEJ mice

The neural activities of the mPFC and striatum play important roles in associative learning [34–36]. It is also reported that methamphetamine and amphetamine cause abnormal activation of the mPFC and striatum as evidenced by an increase in c-Fos expression [37–41]. To further investigate the mechanism underlying the vulnerability to methamphetamine in *Arhgap10* S490P/NHEJ mice, we evaluated c-Fos expression levels in the mPFC and striatum after methamphetamine treatment. Even a low methamphetamine dose of 0.3 mg/kg i.p. significantly increased the number of c-Fos–positive cells in the mPFC and striatum of *Arhgap10* S490P/NHEJ mice (Fig. 5A, B, C, D). Methamphetamine-induced c-Fos expression in *Arhgap10* S490P/NHEJ mice was significantly suppressed by pretreatment with fasudil at a dose of 20 mg/kg i.p. in the mPFC (Fig. 5A, B) (Fig. 5B, mPFC, 2-way ANOVA, methamphetamine: $F(1, 53) = 11.30$, $P = 0.0014$, fasudil: $F(1, 53) = 22.75$, $P < 0.0001$, methamphetamine × fasudil: $F(1, 53) = 6.040$, $P = 0.0173$), but not in the striatum (Fig. 5C, D) (Fig. 5D, striatum, Kruskal–Wallis test, $P = 0.0023$). In WT mice, methamphetamine at 0.3 mg/kg i.p. had no significant effects on the number of c-Fos–positive cells in the mPFC or striatum, while fasudil (20 mg/kg, i.p.) decreased the number of c-Fos–positive cells only in the saline-pretreated group, and only in the striatum and not the mPFC (Fig. S1A, B, C, D) (Fig. S1B, Kruskal–Wallis test, $P = 0.1867$; Fig. S1D, Kruskal–Wallis test,

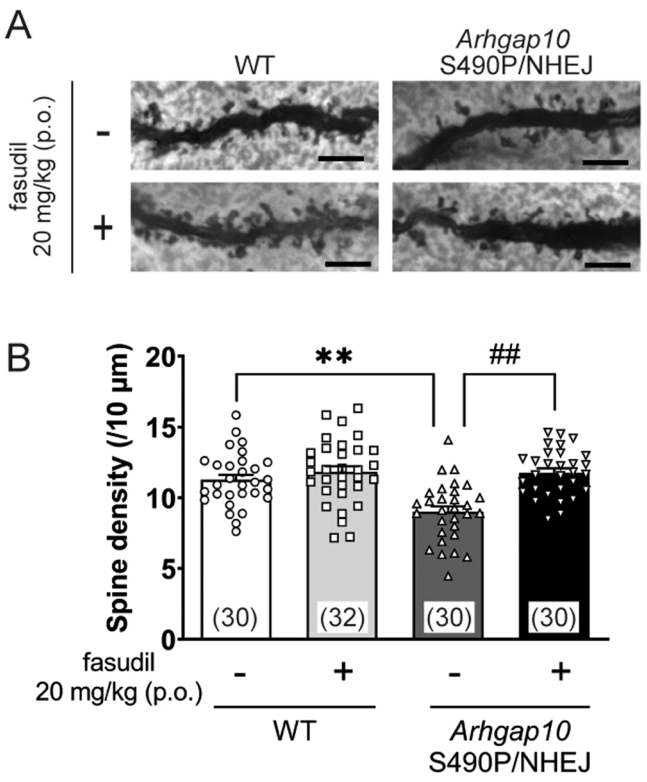

Fig. 3. The effect of fasudil on spine density in the mPFC of *Arhgap10* S490P/NHEJ mice A. Representative images of dendric spines (scale bar indicates 5 μm). **B.** Spine density of layer 2/3 pyramidal neurons in the mPFC of *Arhgap10* S490P/NHEJ mice or WT mice after fasudil (20 mg/kg, p.o.) treatment for 7 days. Data represent the mean ± SEM (n = 30–32 dendrites in each of 5 mice per group (6–7 dendrites per mouse)) and were analyzed by Tukey's multiple comparison test. $^{**}P < 0.01$ compared with WT mice and $^{\#\#}P < 0.01$ compared with the vehicle group.

P = 0.0171). These results suggest that Rho-kinase is involved in the vulnerability to methamphetamine in the mPFC of *Arhgap10* S490P/NHEJ mice.

4. Discussion

We previously reported that RhoA/Rho-kinase signaling was activated in the brain of *Arhgap10* S490P/NHEJ mice, whose mutations mimic those in *ARHGAP10* identified by genome-wide CNV analysis of Japanese patients with schizophrenia [22]. Furthermore, the model mice show an abnormal spine density in the mPFC and methamphetamine-induced cognitive impairment in the visual discrimination task [21,22]. Here, we demonstrated that a brain-permeable Rho-kinase inhibitor, fasudil, suppressed the phosphorylation levels of MYPT1 in the striatum and mPFC in *Arhgap10* S490P/NHEJ mice (Figs. 1, 2). Notably, fasudil ameliorated the reduced spine density in the mPFC (Fig. 3) and the methamphetamine-induced cognitive impairment in the visual discrimination task (Fig. 4) in these mice. These results suggest that Rho-kinase is involved in the reduced spine density in the mPFC as well as in the cognitive impairment in *Arhgap10* S490P/NHEJ mice.

We initially demonstrated that fasudil (20 mg/kg, i.p.) suppressed the phosphorylation levels of MYPT1 (Thr696) in the striatum and NAc of *Arhgap10* S490P/NHEJ mice without affecting the total levels of MYPT1 (Fig. 1A–F). ARHGAP10, a member of the RhoGAP superfamily, negatively regulates small GTPase RhoA [23,24]. Rho-kinase activated by RhoA directly phosphorylates MYPT1 at Thr696 and MLC. Phosphorylated MYPT1 at Thr696 inhibits MLC phosphatase, leading to sustained phosphorylation of MLC [32,42,43]. We previously reported that the systemic administration of fasudil increased the brain concentrations of fasudil and hydroxyfasudil, an active metabolite of fasudil, above their respective Ki values for Rho-kinase [28]. Furthermore, our results confirmed those of a previous study showing that systemic administration of hydroxyfasudil suppressed the phosphorylation levels of MYPT1 (Thr696) in mouse brains [44]. These results suggest that fasudil crosses the blood–brain barrier and inhibits Rho-kinase in the brain after systemic administration. We demonstrated that the ratio of pMYPT1 (Thr696) and NeuN double-positive neurons to NeuN-positive neurons in the mPFC of *Arhgap10* S490P/NHEJ mice was higher than that in WT mice, and fasudil (20 mg/kg, i.p.) decreased it (Fig. 2 C). However, we failed to detect significant differences between *Arhgap10* S490P/NHEJ mice and WT mice regarding pMYPT1 levels in brain lysates of the mPFC (Fig. 1G–I). Rho-kinase was reported to be expressed in neurons, glial cells, and endothelial cells in the mouse brain and in post-mortem human brain tissue [45–47]. Some authors identified RhoA/Rho-kinase activity in rat cortical synaptosomes and spines [48,49]. Of note, most pMYPT1 immunoreactivity in this study was observed in NeuN-positive neurons in the mPFC regardless of *Arhgap10* mutations and fasudil treatment (Fig. 2B). This indicates that in *Arhgap10* S490P/NHEJ mice, activation of Rho-kinase occurs mainly in mPFC neurons and that RhoA/Rho-kinase signaling is activated in the striatum, NAc, and mPFC.

Next, we demonstrated that fasudil restored the decreased spine density of layer 2/3 pyramidal neurons in the mPFC of *Arhgap10* S490P/NHEJ mice (Fig. 3). RhoA/Rho-kinase signaling regulates actin cytoskeleton organization to promote spine loss and neurite retraction in neurons [26,27,50–52]. Indeed, we previously reported that the Rho-kinase inhibitor Y-27632 restored the impairment of neurite elongation in tyrosine hydroxylase–positive neurons that had differentiated from induced pluripotent stem cells derived from a schizophrenia patient with *ARHGAP10* mutations [21]. Moreover, our data were consistent with previous studies showing that inhibitors of RhoA or Rho-kinase improved abnormal spine morphology in various model mice [53–55]. The selective RhoA inhibitor Rhosin enhanced spine density in the NAc in socially defeated mice [53]. Fasudil restored the decreased spine density in cortical pyramidal neurons of Cdh (a cofactor of the anaphase-promoting complex/cyclosome ubiquitin ligase) knock-out mice and the abnormal dendritic spine remodeling in CA1 of the hippocampus of mice exposed to traumatic brain injury [54,55]. Therefore, these results suggest that Rho-kinase is involved in the decreased spine density of cortical neurons in *Arhgap10* S490P/NHEJ mice. On the other hand, our study indicated that fasudil had no effects on spine density in WT mice (Fig. 3), while Y-27632 was reported to increase dendritic spine density in hippocampal primary neurons of WT mice [56]. Under our experimental conditions, the brain concentrations of fasudil and hydroxyfasudil following systemic administration were much lower than those in in vitro experiments [28], which may have prevented us from detecting any changes in spine density in WT mice.

Arhgap10 S490P/NHEJ mice are vulnerable to methamphetamine, and even low-dose methamphetamine treatment impairs visual discrimination in these mice but not in WT mice [22]. The mutant mice also show enhanced methamphetamine-induced hyperlocomotion compared with WT mice [21]. Cognitive dysfunction is one of the core symptoms of schizophrenia, but is only minimally ameliorated by current antipsychotics [14]. Recently, touchscreen paradigms have been used to bridge the translational gap between rodents and humans in terms of assessing cognition and drug screening for cognitive disorders [57,58]. In this study, we demonstrated that fasudil completely rescued the methamphetamine-induced impairment of a touchscreen–based discrimination task in *Arhgap10* S490P/NHEJ mice (Fig. 4). We confirmed that fasudil at a dose of 20 mg/kg i.p. did not affect the performance of saline-treated WT mice in the visual discrimination task [33]. Therefore, our findings suggest that Rho-kinase contributes to the methamphetamine-induced cognitive impairment in *Arhgap10* S490P/NHEJ mice. Our data are highly consistent with our previous

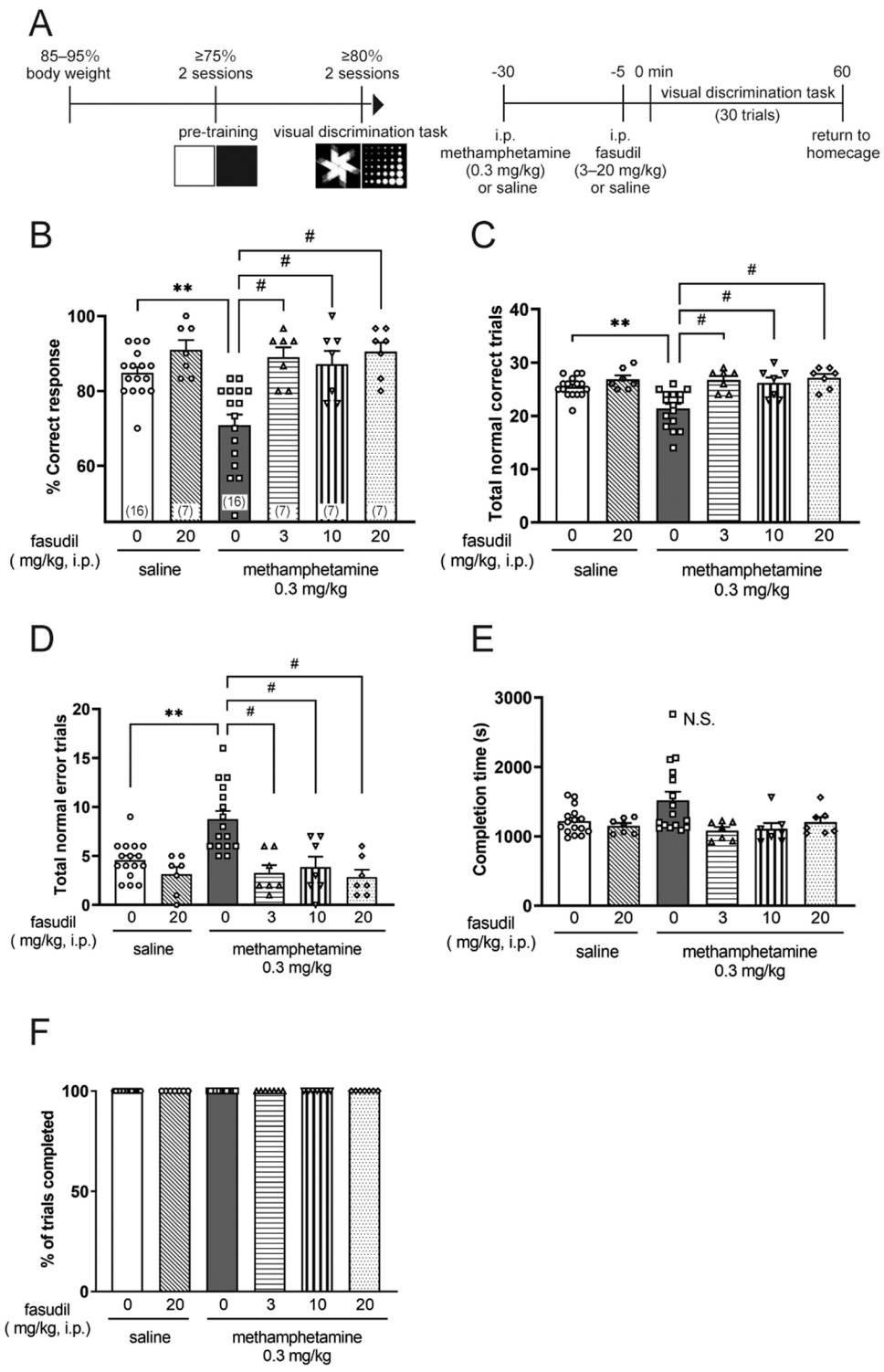

Fig. 4. The effect of fasudil on the methamphetamine-induced impairment of visual discrimination in *Arhgap10* S490P/NHEJ mice A. The protocols of the visual discrimination task (left) and drug treatment (right). B. Percentage of correct responses, C. Total normal correct trials, D. Total normal error trials, E. Completion time, and F. Percentage of trials completed in the visual discrimination task. The animals were treated with methamphetamine (0.3 mg/kg, i.p.) and fasudil (20 mg/kg, i.p.) 30 min and 5 min before the task, respectively. Data represent the mean ± SEM (n = 7–16 mice per group) and were analyzed by Tukey's multiple comparison test. * *P < 0.01 compared with WT mice and #P < 0.05 compared with the vehicle group.

study showing that fasudil restored impaired cognitive function in a MK-801–treated pharmacologic mouse model of schizophrenia [28]. In addition, other groups have reported that fasudil enhances action–outcome memory and blocks cocaine-induced behavioral inflexibility in mice [59,60]. Importantly, fasudil showed beneficial effects on neuropathological changes in spine morphology and cognitive function in adult *Arhgap10* S490P/NHEJ mice (Figs. 3, 4). Thus, Rho-kinase could be a potential therapeutic target of schizophrenia during adulthood, when symptoms have already developed.

Finally, we found that methamphetamine at a dose of 0.3 mg/kg, which impaired visual discrimination in *Arhgap10* S490P/NHEJ mice without affecting WT mice, increased neuronal activity in the mPFC and striatum of *Arhgap10* S490P/NHEJ mice as evidenced by c-Fos expression (Fig. 5). In contrast, methamphetamine at the same dose did not affect c-Fos expression in WT mice (Fig. S1). We previously reported that *Arhgap10* S490P/NHEJ mice showed a significant increase in the number of c-Fos–positive cells in the striatum and NAc core compared with WT mice after methamphetamine treatment [22]. These suggest that methamphetamine at the dose used in the visual discrimination task can induce abnormal neuronal activation in the mPFC and striatum in

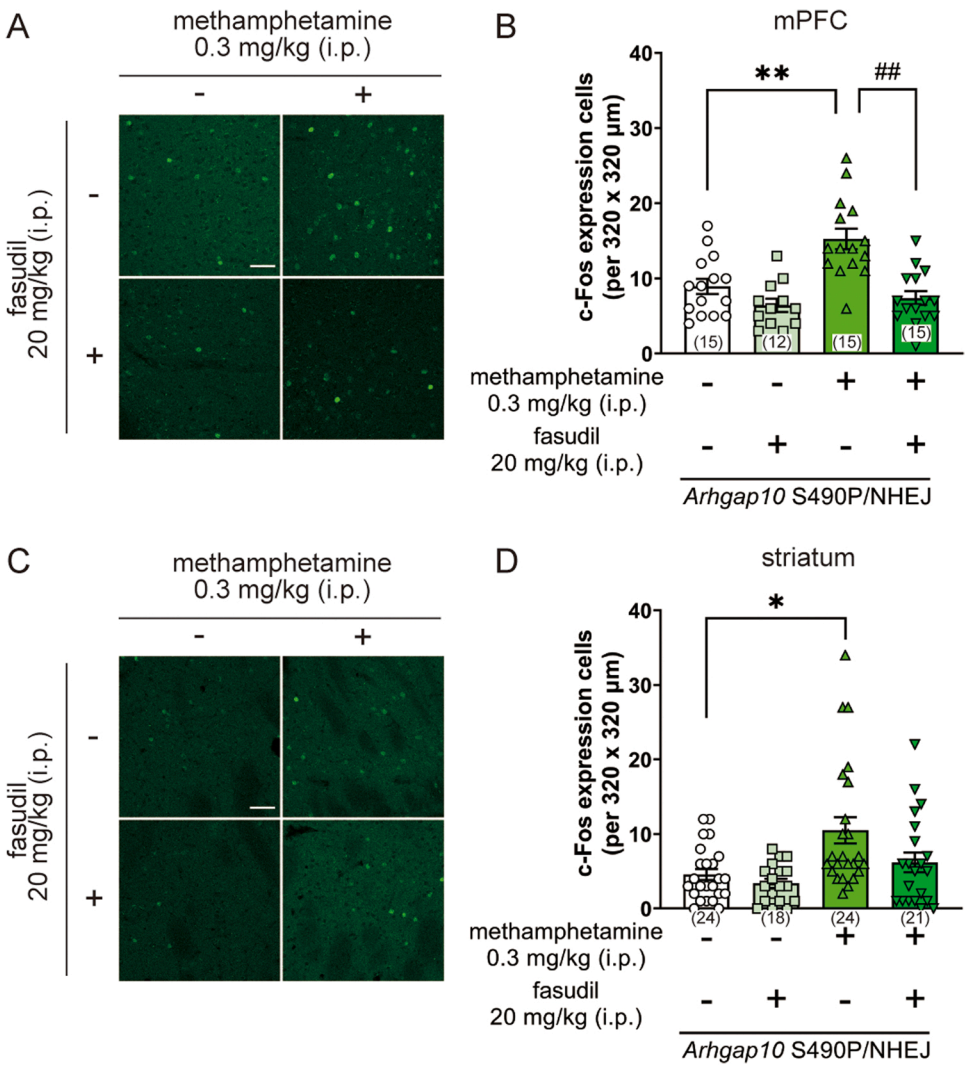

Fig. 5. The effect of fasudil on the number of c-Fos–positive cells in the mPFC and striatum of *Arhgap10* S490P/NHEJ mice A, C. Representative images of c-Fos immunoreactivity in the mPFC (A) and striatum (C) of *Arhgap10* S490P/NHEJ mice (scale bar indicates 50 μm). B, D. Number of c-Fos–positive cells in the mPFC (B) and striatum (D) of *Arhgap10* S490P/NHEJ mice. The animals were treated with methamphetamine (0.3 mg/kg, i.p.) and fasudil (20 mg/kg, i.p.) 150 min and 125 min before perfusion, respectively. Data represent the mean ± SEM (n = 12–15 slices in each of 4–5 mice per group (3 slices per mouse) in the mPFC (B), and n = 18–24 slices in each of 6–8 mice per group (3 slices per mouse) in the striatum (D)) and were analyzed by Tukey's multiple comparison test or Dunn's multiple comparisons test. $^{*}P < 0.05$, $^{**}P < 0.01$ compared with the saline-saline–treated group and $^{\#\#}P < 0.01$ compared with the methamphetamine-saline–treated group.

Arhgap10 S490P/NHEJ mice, but not in WT mice. Importantly, we observed that fasudil suppressed the increased number of c-Fos–positive cells in the mPFC but not the striatum of *Arhgap10* S490P/NHEJ mice (Fig. 5), suggesting that Rho-kinase is associated with methamphetamine-induced neuronal activation in the mPFC of *Arhgap10* S490P/NHEJ mice. Methamphetamine increases dopamine release in the mPFC and striatum and facilitates the transport of N-methyl-D-aspartate receptors (NMDA-Rs) to postsynaptic subcellular compartments, thereby triggering Ca^{2+}-dependent ERK activation via dopamine D1 receptors [61,62]. NMDA-Rs stimulation activates RhoA/Rho-kinase signaling, which in turn induces Ras-ERK signaling and morphological changes in spines by phosphorylating synaptic Ras-GTPase activating protein 1 (SynGAP1) [63,64]. Thus, inhibition of Rho-kinase may suppress neuronal activity in the mPFC by inactivating Ras-ERK signaling. In the visual discrimination task, the corticostriatal circuits play important roles in learning [65]. In particular, the neuronal activity in the mPFC is stimulated by the cue–response association and rule shifting [34,66,67]. Local injection of Y-27632 into the mPFC rescued the methamphetamine (1 mg/kg, i.p.)-induced impairment in the visual discrimination task in WT mice [33]. These data suggest that methamphetamine-induced abnormal neuronal activation in the mPFC via Rho-kinase is associated with methamphetamine-induced cognitive impairment in *Arhgap10* S490P/NHEJ mice.

We could not detect basal differences in cognitive function or neuronal activity between WT and *Arhgap10* S490P/NHEJ mice (Figs. 4, 5) [22], although spine density in the mPFC was significantly decreased in *Arhgap10* S490P/NHEJ mice. This deficit was significantly restored by fasudil treatment, while fasudil had no effect on spine density in WT mice (Fig. 3). These findings suggest that decreased basal spine density in the mPFC may not be directly related to cognitive impairment in *Arhgap10* S490P/NHEJ mice. Alternatively, the touchscreen-based simple visual discrimination test and reversal learning may not be sensitive enough to detect potential basal cognitive deficits in *Arhgap10* S490P/NHEJ mice. Of note, mice deficient in the Abl-related gene kinase, which acts through p190RhoGAP to inhibit RhoA, show decreased basal spine density in the PFC and a vulnerability to cocaine, and exhibit defective cocaine-induced spine plasticity [60,68,69]. Accordingly, to understand the mechanism of fasudil it is important to investigate its effect on dendritic spine plasticity induced by the visual discrimination task after methamphetamine treatment.

An important limitation of our work is the use of fasudil to inhibit Rho-kinase. Fasudil is widely used as Rho-kinase inhibitor and shows inhibitory activity against Rho-kinase 1 (IC_{50} 0.36 μM) [70] and Rho-kinase 2 (IC_{50} 0.158 μM) [71]. However, fasudil is reported to inhibit other kinases such as PKA (IC_{50} 4.58 μM), PKG (IC_{50} 1.65 μM), and CaMKII (IC_{50} 6.70 μM) [71]. Therefore, this study cannot exclude the possibility that other candidate molecules are involved in the effects of fasudil. To obtain solid evidence for the pathological role of Rho-kinase in *Arhgap10* S490P/NHEJ mice, studies using genetic tools such as conditional Rho-kinase knockout mice are required.

5. Conclusion

In conclusion, our results suggest that Rho-kinase plays a significant role in the neuropathological changes in spine morphology as well as in the vulnerability to methamphetamine in *Arhgap10* S490P/NHEJ mice. Targeting RhoA/Rho-kinase signaling may provide new therapeutic approaches for the treatment of schizophrenia patients with *Arhgap10* gene mutations.

Funding information

This study was supported by AMED (JP21wm0425007, JP21wm0425017, JP19dm0207075), Japan; Japan Society for the Promotion of Science (JSPS) KAKENHI (20H03428, 20K07082), Japan; SRF, Japan; Takeda Science Foundation, Japan; Toyoaki Scholarship Foundation, Japan.

CRediT authorship contribution statement

Rinako Tanaka: Conceptualization, Methodology, Investigation, Formal analysis, Writing – original draft, Funding acquisition. **Jingzhu Liao:** Methodology, Investigation, Formal analysis. **Kazuhiro Hada:** Methodology, Investigation, Formal analysis, Writing – review & editing. **Daisuke Mori:** Resources. **Taku Nagai:** Writing – review & editing, Funding acquisition, Supervision. **Tetsuo Matsuzaki:** Writing – review & editing, Supervision. **Toshitaka Nabeshima:** Writing – review & editing, Supervision. **Kozo Kaibuchi:** Writing – review & editing, Funding acquisition, Supervision. **Norio Ozaki:** Writing – review & editing, Funding acquisition, Supervision. **Hiroyuki Mizoguchi:** Writing – review & editing, Funding acquisition, Supervision. **Kiyofumi Yamada:** Writing – review & editing, Project administration, Funding acquisition, Supervision.

Declaration of Competing Interest

This study was funded in part by Sumitomo Pharma Co., Ltd.

Data Availability

Data will be made available on request.

Acknowledgments

Fasudil hydrochloride was kindly provided by Asahikasei Co., Ltd. (Tokyo, Japan). The authors wish to acknowledge the Division for Medical Research Engineering, Nagoya University Graduate School of Medicine, for the use of a BZ9000 bright-field microscopic (KEYENCE) and a cryostat (CM3050S; Leica), and the staff of the Division of Experimental Animals, Nagoya University Graduate School of Medicine, for their technical support. This work was financially supported by JST SPRING, Grant Number JPMJSP2125. One of the authors (R.T.) would like to take this opportunity to thank the Interdisciplinary Frontier Next-Generation Researcher Program of the Tokai Higher Education and Research System.

Author Contributions

R.T. wrote the main text and prepared most of the figures; R.T. performed immunohistochemistry and Golgi staining and analyzed the data; JZ.L. performed behavioral experiments and analyzed the data; K. H. performed western blotting and analyzed the data; D.M. generated the *Arhgap10* S490P/NHEJ mice; Ta.N., T. M., To.N., K.K., N.O., H.M., and K.Y. supervised the overall project. All authors have carefully read the paper and approved the final manuscript.

Appendix A. Supporting information

Supplementary data associated with this article can be found in the online version at doi:10.1016/j.phrs.2022.106589.

References

[1] N. Gogtay, et al., Age of onset of schizophrenia: perspectives from structural neuroimaging studies, Schizophr. Bull. 37 (3) (2011) 504–513.
[2] P. Stepnicki, M. Kondej, A.A. Kaczor, Current concepts and treatments of schizophrenia, Molecules 23 (8) (2018).
[3] C.G.J. Guerrin, et al., The dual hit hypothesis of schizophrenia: evidence from animal models, Neurosci. Biobehav. Rev. 131 (2021) 1150–1168.
[4] I. Kushima, et al., Cross-disorder analysis of genic and regulatory copy number variations in bipolar disorder, schizophrenia, and autism spectrum disorder, Biol. Psychiatry 92 (5) (2022) 362–374.
[5] I. Kushima, et al., Comparative analyses of copy-number variation in autism spectrum disorder and schizophrenia reveal etiological overlap and biological insights, Cell Rep. 24 (11) (2018) 2838–2856.
[6] A. Jutla, J. Foss-Feig, J. Veenstra-VanderWeele, Autism spectrum disorder and schizophrenia: an updated conceptual review, Autism Res. 15 (3) (2022) 384–412.
[7] H. Li, et al., Methamphetamine enhances the development of schizophrenia in first-degree relatives of patients with schizophrenia, Can. J. Psychiatry 59 (2) (2014) 107–113.
[8] J.A. Lieberman, J.M. Kane, J. Alvir, Provocative tests with psychostimulant drugs in schizophrenia, Psychopharmacology 91 (4) (1987) 415–433.
[9] C. Curran, N. Byrappa, A. McBride, Stimulant psychosis: systematic review, Br. J. Psychiatry 185 (2004) 196–204.
[10] M. Laruelle, et al., Single photon emission computerized tomography imaging of amphetamine-induced dopamine release in drug-free schizophrenic subjects, Proc. Natl. Acad. Sci. USA 93 (17) (1996) 9235–9240.
[11] Q. Wu, J. Huang, R. Wu, Drugs based on NMDAR hypofunction hypothesis in schizophrenia, Front Neurosci. 15 (2021), 641047.
[12] R.S. Kahn, I.E. Sommer, The neurobiology and treatment of first-episode schizophrenia, Mol. Psychiatry 20 (1) (2015) 84–97.
[13] A. Lin, et al., Neurocognitive predictors of functional outcome two to 13 years after identification as ultra-high risk for psychosis, Schizophr. Res. 132 (1) (2011) 1–7.
[14] P.D. Harvey, et al., Cognitive dysfunction in schizophrenia: An expert group paper on the current state of the art, Schizophr. Res. Cogn. 29 (2022), 100249.
[15] O.D. Howes, et al., Neuroimaging in schizophrenia: an overview of findings and their implications for synaptic changes, Neuropsychopharmacology (2022).
[16] J.R. Glausier, D.A. Lewis, Dendritic spine pathology in schizophrenia, Neuroscience 251 (2013) 90–107.
[17] K. Broadbelt, W. Byne, L.B. Jones, Evidence for a decrease in basilar dendrites of pyramidal cells in schizophrenic medial prefrontal cortex, Schizophr. Res. 58 (1) (2002) 75–81.
[18] G.T. Konopaske, et al., Prefrontal cortical dendritic spine pathology in schizophrenia and bipolar disorder, JAMA Psychiatry 71 (12) (2014) 1323–1331.
[19] K. Runge, C. Cardoso, A. de Chevigny, Dendritic spine plasticity: function and mechanisms, Front. Synaptic Neurosci. 12 (2020) 36.
[20] Z. Yan, B. Rein, Mechanisms of synaptic transmission dysregulation in the prefrontal cortex: pathophysiological implications, Mol. Psychiatry 27 (1) (2022) 445–465.
[21] M. Sekiguchi, et al., ARHGAP10, which encodes Rho GTPase-activating protein 10, is a novel gene for schizophrenia risk, Transl. Psychiatry 10 (1) (2020) 247.
[22] K. Hada, et al., Mice carrying a schizophrenia-associated mutation of the Arhgap10 gene are vulnerable to the effects of methamphetamine treatment on cognitive function: association with morphological abnormalities in striatal neurons, Mol. Brain 14 (1) (2021) 21.
[23] N. Mosaddeghzadeh, M.R. Ahmadian, The RHO family GTPases: mechanisms of regulation and signaling, Cells 10 (7) (2021).
[24] L. Liu, et al., ARHGAP10 inhibits the proliferation and metastasis of CRC cells via blocking the activity of RhoA/AKT signaling pathway, Onco Targets Ther. 12 (2019) 11507–11516.
[25] K. Riento, A.J. Ridley, Rocks: multifunctional kinases in cell behaviour, Nat. Rev. Mol. Cell Biol. 4 (6) (2003) 446–456.
[26] T. Sarowar, A.M. Grabrucker, Rho GTPases in the amygdala-a switch for fears? Cells 9 (9) (2020).
[27] S.E. Newey, et al., Rho GTPases, dendritic structure, and mental retardation, J. Neurobiol. 64 (1) (2005) 58–74.
[28] S. Takase, et al., Antipsychotic-like effects of fasudil, a Rho-kinase inhibitor, in a pharmacologic animal model of schizophrenia, Eur. J. Pharm. 931 (2022), 175207.
[29] M. Isshiki, et al., Enhanced synapse remodelling as a common phenotype in mouse models of autism, Nat. Commun. 5 (2014) 4742.
[30] M. Sawahata, et al., Microinjection of Reelin into the mPFC prevents MK-801-induced recognition memory impairment in mice, Pharm. Res. 173 (2021), 105832.
[31] Y. Kawano, et al., Phosphorylation of myosin-binding subunit (MBS) of myosin phosphatase by Rho-kinase in vivo, J. Cell Biol. 147 (5) (1999) 1023–1038.
[32] M. Amano, et al., Identification of the kinase-substrate recognition interface between MYPT1 and Rho-Kinase, Biomolecules 12 (2) (2022).
[33] J. Liao et al., Rho kinase inhibitors ameliorate acute methamphetamine-induced cognitive impairment through the cortico-striatal circuit in mice [accessed

November 22, 2022]Author, [Prepr.] September 28, 2022 doi: 10.22541/au.166439569.90753669/v1.
[34] W.F. Asaad, G. Rainer, E.K. Miller, Neural activity in the primate prefrontal cortex during associative learning, Neuron 21 (6) (1998) 1399–1407.
[35] M. Zheng, et al., Choice-dependent cross-modal interaction in the medial prefrontal cortex of rats, Mol. Brain 14 (1) (2021) 13.
[36] H.C. Bergstrom, et al., Dorsolateral striatum engagement interferes with early discrimination learning, Cell Rep. 23 (8) (2018) 2264–2272.
[37] B.C. Shyu, et al., Methamphetamine and modulation functionality of the prelimbic cortex for developing a possible treatment of Alzheimer's disease in an animal model, Front. Aging Neurosci. 13 (2021), 751913.
[38] B. González, et al., The effects of single-dose injections of modafinil and methamphetamine on epigenetic and functional markers in the mouse medial prefrontal cortex: potential role of dopamine receptors, Prog. Neuropsychopharmacol. Biol. Psychiatry 88 (2019) 222–234.
[39] E. Martín-García, et al., Frequency of cocaine self-administration influences drug seeking in the rat: optogenetic evidence for a role of the prelimbic cortex, Neuropsychopharmacology 39 (10) (2014) 2317–2330.
[40] N.B. Gross, P.C. Duncker, J.F. Marshall, Cortical ionotropic glutamate receptor antagonism protects against methamphetamine-induced striatal neurotoxicity, Neuroscience 199 (2011) 272–283.
[41] A.N. Mead, et al., AMPA-receptor involvement in c-fos expression in the medial prefrontal cortex and amygdala dissociates neural substrates of conditioned activity and conditioned reward, Eur. J. Neurosci. 11 (11) (1999) 4089–4098.
[42] M.E. Grassie, et al., The myosin phosphatase targeting protein (MYPT) family: a regulated mechanism for achieving substrate specificity of the catalytic subunit of protein phosphatase type 1delta, Arch. Biochem. Biophys. 510 (2) (2011) 147–159.
[43] T.M. Seccia, et al., ROCK (RhoA/Rho Kinase) in cardiovascular-renal pathophysiology: a review of new advancements, J. Clin. Med. 9 (5) (2020).
[44] J.H. Lee, et al., Selective ROCK2 inhibition in focal cerebral ischemia, Ann. Clin. Transl. Neurol. 1 (1) (2014) 2–14.
[45] M. Iizuka, et al., Distinct distribution and localization of Rho-kinase in mouse epithelial, muscle and neural tissues, Cell Struct. Funct. 37 (2) (2012) 155–175.
[46] K.A. Saal, et al., Altered expression of growth associated protein-43 and Rho kinase in human patients with Parkinson's disease, Brain Pathol. 27 (1) (2017) 13–25.
[47] B. Niego, et al., Selective inhibition of brain endothelial Rho-kinase-2 provides optimal protection of an in vitro blood-brain barrier from tissue-type plasminogen activator and plasmin, PLoS One 12 (5) (2017), e0177332.
[48] B. Lontay, et al., Protein phosphatase-1M and Rho-kinase affect exocytosis from cortical synaptosomes and influence neurotransmission at a glutamatergic giant synapse of the rat auditory system, J. Neurochem. 123 (1) (2012) 84–99.
[49] N.G. Hedrick, et al., Rho GTPase complementation underlies BDNF-dependent homo- and heterosynaptic plasticity, Nature 538 (7623) (2016) 104–108.
[50] W. Ba, J. van der Raadt, N. Nadif Kasri, Rho GTPase signaling at the synapse: implications for intellectual disability, Exp. Cell Res. 319 (15) (2013) 2368–2374.
[51] S. Hartmann, A.J. Ridley, S. Lutz, The function of rho-associated kinases ROCK1 and ROCK2 in the pathogenesis of cardiovascular disease, Front. Pharm. 6 (2015) 276.
[52] O. Martin-Camara, et al., Emerging targets in drug discovery against neurodegenerative diseases: Control of synapsis disfunction by the RhoA/ROCK pathway, Eur. J. Med. Chem. 225 (2021), 113742.
[53] T.C. Francis, et al., The selective RhoA inhibitor rhosin promotes stress resiliency through enhancing D1-medium spiny neuron plasticity and reducing hyperexcitability, Biol. Psychiatry 85 (12) (2019) 1001–1010.
[54] V. Bobo-Jiménez, et al., APC/C(Cdh1)-Rock2 pathway controls dendritic integrity and memory, Proc. Natl. Acad. Sci. USA 114 (17) (2017) 4513–4518.
[55] S. Mulherkar, et al., RhoA-ROCK inhibition reverses synaptic remodeling and motor and cognitive deficits caused by traumatic brain injury, Sci. Rep. 7 (1) (2017) 10689.
[56] S.A. Swanger, et al., ROCK1 and ROCK2 inhibition alters dendritic spine morphology in hippocampal neurons, Cell Logist. 5 (4) (2015), e1133266.
[57] D.L. Spark, et al., Beyond antipsychotics: a twenty-first century update for preclinical development of schizophrenia therapeutics, Transl. Psychiatry 12 (1) (2022) 147.
[58] J. Nithianantharajah, et al., Bridging the translational divide: identical cognitive touchscreen testing in mice and humans carrying mutations in a disease-relevant homologous gene, Sci. Rep. 5 (2015) 14613.
[59] A.M. Swanson, L.M. DePoy, S.L. Gourley, Inhibiting Rho kinase promotes goal-directed decision making and blocks habitual responding for cocaine, Nat. Commun. 8 (1) (2017) 1861.
[60] L.M. DePoy, et al., Induction and blockade of adolescent cocaine-induced habits, Biol. Psychiatry 81 (7) (2017) 595–605.
[61] M. Salery, et al., From signaling molecules to circuits and behaviors: cell-type-specific adaptations to psychostimulant exposure in the striatum, Biol. Psychiatry 87 (11) (2020) 944–953.
[62] C.H. Trepanier, M.F. Jackson, J.F. MacDonald, Regulation of NMDA receptors by the tyrosine kinase Fyn, FEBS J. 279 (1) (2012) 12–19.
[63] M. Wu, et al., Rho-Rho-Kinase regulates Ras-ERK signaling through SynGAP1 for dendritic spine morphology, Neurochem. Res. (2022).
[64] T. Nakazawa, et al., Regulation of dendritic spine morphology by an NMDA receptor-associated Rho GTPase-activating protein, p250GAP, J. Neurochem. 105 (4) (2008) 1384–1393.
[65] J.L. Brigman, et al., GluN2B in corticostriatal circuits governs choice learning and choice shifting, Nat. Neurosci. 16 (8) (2013) 1101–1110.
[66] I. Lee, J.Y. Shin, Medial prefrontal cortex is selectively involved in response selection using visual context in the background, Learn Mem. 19 (6) (2012) 247–250.
[67] A. Izquierdo, et al., The neural basis of reversal learning: An updated perspective, Neuroscience 345 (2017) 12–26.
[68] S.L. Gourley, A.J. Koleske, J.R. Taylor, Loss of dendrite stabilization by the Abl-related gene (Arg) kinase regulates behavioral flexibility and sensitivity to cocaine, Proc. Natl. Acad. Sci. USA 106 (39) (2009) 16859–16864.
[69] S.L. Gourley, et al., Arg kinase regulates prefrontal dendritic spine refinement and cocaine-induced plasticity, J. Neurosci. 32 (7) (2012) 2314–2323.
[70] Y. Yao, et al., Discovery of novel N-substituted prolinamido indazoles as potent rho kinase inhibitors and vasorelaxation agents, Molecules 22 (10) (2017).
[71] M. Tamura, et al., Development of specific Rho-kinase inhibitors and their clinical application, Biochim. Biophys. Acta 1754 (1–2) (2005) 245–252.